Journal Pre-proof

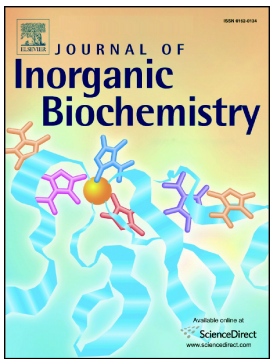

New copper complexes inducing bimodal death through apoptosis and autophagy in A549 cancer cells

Noor Shad Gul, Taj-Malook Khan, Ming Chen, Ke-Bin Huang, Cheng Hou, Muhammad Iqbal Choudhary, Hong Liang, Zhen-Feng Chen

PII: S0162-0134(20)30288-9

DOI: https://doi.org/10.1016/j.jinorgbio.2020.111260

Reference: JIB 111260

To appear in: *Journal of Inorganic Biochemistry*

Received date: 11 July 2020

Revised date: 13 September 2020

Accepted date: 21 September 2020

Please cite this article as: N.S. Gul, T.-M. Khan, M. Chen, et al., New copper complexes inducing bimodal death through apoptosis and autophagy in A549 cancer cells, *Journal of Inorganic Biochemistry* (2018), https://doi.org/10.1016/j.jinorgbio.2020.111260

This is a PDF file of an article that has undergone enhancements after acceptance, such as the addition of a cover page and metadata, and formatting for readability, but it is not yet the definitive version of record. This version will undergo additional copyediting, typesetting and review before it is published in its final form, but we are providing this version to give early visibility of the article. Please note that, during the production process, errors may be discovered which could affect the content, and all legal disclaimers that apply to the journal pertain.

© 2018 Published by Elsevier.

New copper complexes inducing bimodal death through apoptosis and autophagy in A549 cancer cells

Noor Shad Gul[1,#], Taj-Malook Khan[1,#], Ming Chen[1], Ke-Bin Huang[1], Cheng Hou[1], Muhammad Iqbal Choudhary[2], Hong Liang[1], and Zhen-Feng Chen[1,*]

[1]State Key Laboratory for Chemistry and Molecular Engineering of Medicinal Resources, School of Chemistry and Pharmacy, Guangxi Normal University, Guilin 541004, P. R. China

[2]International Center for Chemical and Biological Sciences, University of Karachi, Karachi-74270, Pakistan

Correspondence to:

Professor Zhen-Feng Chen

State Key Laboratory for Chemistry and Molecular Engineering of Medicinal Resources, School of Chemistry and Pharmacy, Guangxi Normal University, 15 Yucai Road, Guilin 541004, P. R. China

Fax: 086-773-2120950

E-mail: chenzf@gxnu.edu.cn (Z.-F. Chen)

Journal Pre-proof

Abstract

Two copper complexes, **Cu1** (CuL^1Cl_2, L^1 = 2-(6,7-dimethoxyisoquinolin-1-yl) aniline) and **Cu2** (CuL^2Cl_2, L^2 = 2-(6-methoxyisoquinolin-1-yl) aniline), were synthesized and characterized. These complexes exhibited high cytotoxic activity toward different cancer cell lines, including the A549 lung cancer cell line, and low cytotoxicity toward normal human cells. Mechanistic studies have shown that these complexes induce bimodal death of cancer cells through apoptosis and autophagy, including the activation of apoptotic and autophagic cell signaling pathways. In addition, **Cu1** and **Cu2** interacted with calf thymus DNA (ct-DNA) via an intercalative binding mode. The different biological behaviors of these copper complexes could be attributed to the presence of electron-donating methoxy groups on the ligands. **Cu1** and **Cu2** effectively inhibited tumor growth in a xenografted mouse model bearing A549 cells but exhibited lower in vivo toxicity than cisplatin. Thus, **Cu1** and **Cu2** can be developed as potential anticancer agents.

Keywords: copper agent; isoquinoline; anticancer activity; apoptosis; autophagy; cell cycle.

Journal Pre-proof

1. Introduction

Transition metal complexes have been used for the treatment of many diseases such as cancer, bacterial infection, and inflammation during the past few decades [1]. In the field of cancer chemotherapy, platinum complexes have attained notable achievements for their clinical applications [2-4]. However, acquired resistance and toxicity cause severe side effects and limit the clinical application of these drugs [5,6]. The side effects are owing to the low selectivity for cancer cells [7].

The metal complexes showing single anticancer mechanism are typically not effective in the treatment of tumors, and they produce drug resistance and toxicity because cancer is a multigenetic and complicated disease [8]. Therefore, to overcome these side effects and multi-drug resistance, the development of multi-targeted anticancer agents is most desirable [10]. At present, drugs with multitargeting capability are highly sought to overcome the drawbacks of single targeting drugs. Transition metal complexes can be designed as multi-targeted anticancer agents [9]. In this regard, copper could be an alternative to platinum because it plays a vital role in cancer treatment [11] as numerous copper complexes have been developed and investigated for anticancer activities. In addition, most of the copper complexes produce cytotoxicity by the generation of reactive oxygen species (ROS) inside the cells that initiated various apoptotic pathways [12-14].

During the past two decades, many copper complexes with different ligands have been synthesized and have shown promising anticancer activities against various cancerous cells. For example, several studies have reported some Cu(II) and Pt(II) complexes with high anticancer and pharmacological activity, having isoquinolines and thiosemicarbazones as ligands [15-22]. Some of these complexes kill cells via multiple action mechanisms, which suggest that the

copper complexes could be developed as multitargeting anticancer agents [23-25]. As these complexes damage the cells through various mechanisms, drug resistance in cells, which is typically shown in drugs with single anticancer mechanism, is evaded [26].

Currently, the design and synthesis of transition metal complexes with organic ligands possessing anticancer activity has been the focus of cancer chemotherapy. This is considered a promising strategy to develop potential anticancer agents because the metal complexes usually possess higher biological activities than the corresponding free organic ligands, and exert a synergistic effect after formation of coordination compounds [27,28]. Isoquinoline alkaloids are commonly found in nature, and they exhibit different kinds of biological and pharmacological activities, such as the inhibition of cellular proliferation and cancer cell growth [29]. Berberrubine, a compound of protoberberine alkaloids, is active against tumors in an animal model [30]. Another isoquinoline alkaloid, [1,3]-dioxolo-[4,5-g]-isoquinoline (papraline), which was isolated from the aerial part of *Fumaria indica*, is considered as a mild analgesic, laxative, and diuretic agent and beneficial for skin scrofulous infection and dyspepsia [31]. Previously, we have reported gold and rhodium complexes with isoquinoline derivatives as ligands which exhibited high anticancer activity [32,33].

Herein, we synthesized and determined the crystal structure and in vitro and in vivo activity of two copper(II) complexes with isoquinoline derivatives as ligands. Bimodal death through apoptosis and autophagy in A549 cells was also investigated. These complexes interacted through various pathways such as apoptosis via the mitochondrial-mediated pathway, apoptosis via the mitogen-activated protein kinase mediated (MAPK) pathway, light chain3 protein II mediated (LC3-II) autophagy, and cell damage through the endoplasmic reticulum stress-mediated pathway.

2. Results and discussion

2.1. Chemistry

2.1.1. Synthesis of ligands

Ligands "L^1" 2-(6,7-dimethoxyisoquinolin-1-yl) aniline and "L^2" 2-(6-methoxyisoquinolin-1-yl) aniline were synthesized using the Bischler–Napieralski method of cyclization of acyl products [34] (Scheme S1).

2.1.2. Preparation and crystal structures of Cu1 and Cu2

Copper complexes were synthesized in sealed glass tubes by mixing L^1 or L^2 with $CuCl_2{\cdot}2H_2O$ in a solvent of dichloromethane and methanol (v:v = 1:1) (Scheme S1). Elemental analysis and infrared spectroscopy (IR) were used for structural characterization. Further confirmation of structures was acquired by single crystal X-ray diffraction analysis. The data of crystallographic analysis and refinement details are listed in Table S1 (Supporting Information). The selected bond lengths and bond angles are shown in Tables S2 and S3 (Supporting Information). Isoquinoline is a bidentate ligand having two nitrogen donors (L^1-N^N and L^2-N^N) bound with copper to form the distorted square planar structure in the geometry of **Cu1** and **Cu2**. The **Cu1** crystallized in the $P2_1/c$ space group, whereas **Cu2** crystallized in the C2/c space group. In **Cu1**, the bond lengths of Cu–N1 and Cu–N2 are 1.9980(19) Å and 2.0993(18) Å, respectively; whereas the bond lengths of Cu–Cl1 and Cu–Cl2 are 2.3400(10) Å and 2.3437(9) Å, respectively. In **Cu2**, the bond lengths of Cu–N1 and Cu–N2 are 2.007(3) Å and 2.061(3) Å, respectively, whereas the bond lengths of Cu–Cl1 and Cu–Cl2 are 2.2679(10) Å and 2.2658(9) Å, respectively (Figs. 1, 2).

[Fig. 1]

[Fig. 2]

2.2. Stability of Cu1 and Cu2

The stability of the copper complexes and ligands in phosphate buffer saline (PBS) solution containing 1% DMSO at pH 7.4 were determined at different time intervals of 0, 4, 12, and 24 h by UV-Vis spectroscopy. Furthermore, purity and stability were also checked by high performance liquid chromatography (HPLC). The data showed that **Cu1** and **Cu2** were stable at the given conditions for 24 h. No blue or red shift was observed in the absorption region of spectra, and there was no new peak either (Figs. S1–S8, Supporting Information).

2.3. In vitro cytotoxicity

To evaluate the in vitro cytotoxicity of **Cu1** and **Cu2** ligands and copper salt against various cancer cell lines, MGC80-3, T-24, SKOV-3, HeLa, A549, BEL-7704, and MDA-MB216 and human normal liver cells HL-7702, a 3-(4,5-dimethylthiazol-2-yl)-2,5-diphenyltetrazolium bromide colorimetric assay (MTT) was performed with cisplatin as the positive control. Table 1 shows the IC_{50} values of these compounds against the tested cancer cells. The copper complexes exhibited higher cytotoxicity than corresponding ligands and copper salt. The IC_{50} value of **Cu1** was 3.05 ± 0.3 μM, whereas that of **Cu2** was 6.04 ± 0.5 μM against the A549 cell lines. It was observed that the cytotoxicity of the copper complexes increased by the coordination of isoquinoline derivative ligands with the copper center. In addition, **Cu1** and L^1 were found to be more cytotoxic than **Cu2** and L^2 likely because of the differences in the position and number of methoxy groups, respectively. As reported by Nussbaum [35] the cytotoxicity of complexes mostly depends on the basicity of amine ligands attached to the metal center. For example, the methoxy group is an electron donor that donates electrons to the ring as a result of which electron density becomes high and affords the most effective complexes. Consequently, in the case of **Cu1**, the substitution with two methoxy groups made this complex more basic than **Cu2**

with one methoxy group. The results were found to be consistent with those obtained for the cellular uptake of both copper(II) complexes. Amongst the tested tumor cell lines, **Cu1** and **Cu2** showed the highest cytotoxicity against A549 cells; therefore, we used A549 to investigate their anticancer mechanisms.

[Table 1]

2.4. Distribution and uptake of Cu1 and Cu2

The effect of a drug can be evaluated by its uptake and distribution in a cell [36]. To examine the distribution of **Cu1** and **Cu2** in different parts of the cell including cytosolic, membrane/particulate, cytoskeletal and nucleic fractions, the cells were incubated, based on the concentration of IC_{50} values with **Cu1** (3 μM) and **Cu2** (6 μM) for 20 h and the content of the metals was measured using inductively coupled plasma mass spectrometry (Fig. 3). With the same quantity of A459 cells (10^6 cells), accumulated content of copper complexes was several times greater than that of the control especially in the cytosolic fraction (**Cu1** 3570 ng, **Cu2** 1830 ng) and membrane fraction (**Cu1** 1850 ng, **Cu2** 1450 ng). In addition, in the cytoskeletal fraction, the accumulation of **Cu1** content was higher than that of **Cu2** (1700 ng and 500 ng, respectively). Comparatively little copper was found in the nucleic fraction. This distribution and uptake of metals is critical for the mechanism of actions in different cellular pathways which control the induction of apoptosis [37]. A more detailed evaluation of the possible action mechanisms of **Cu1** and **Cu2** was subsequently conducted.

[Fig. 3]

2.5. Anticancer mechanism of Cu1 and Cu2

2.5.1. Induction of apoptosis by arresting the cell cycle

Journal Pre-proof

The process of apoptosis is exploited as an antitumor mechanism because it is dysregulated in cancer cells. Apoptosis is a highly controlled and conserved process which removes unwanted and abnormal cells during the growth of multicellular organisms [38,39]. To investigate the effects of **Cu1** (1.5, 3.0, 6.0 μM) and **Cu2** (3.0, 6.0, 12.0 μM) on the triggering of apoptosis in A549 cells, after 24-h treatment, the cells were stained with annexin V and propidium iodide and analyzed using flow cytometry. As shown in Figs. 4, S9, S10, the induction of early and late apoptosis showed a dose-dependent increase after treatment with **Cu1** and **Cu2**. The proportions of cells in early and late apoptosis were 1.8% and 4.3%, respectively, in the control. However, this increased to 14.2% and 26.1%, respectively, after treatment with 6.0 μM **Cu1** and 14.4% and 24.3%, respectively, after treatment with 12.0 μM **Cu1**. The extent of apoptosis induction by **Cu1** was greater than that by **Cu2**. As expected, we found that pro-apoptotic proteins, such as Bcl-2-associated X protein (Bax) and Bcl-2 antagonist / killer protein (Bak), were upregulated as compared to that in the control, whereas anti-apoptotic proteins, such as B-cell lymphoma 2 (Bcl-2) and B-cell leukemia xL (Bcl-xL), were down-regulated (Fig. S11).

We further examined the activation of caspases. To this end, A549 cells were exposed to **Cu1** (3.0 μM) and **Cu2** (3.0 μM), and analyzed using flow cytometry after 24 h. As shown in Fig. 5, the levels of caspase-3 were increased from 0.01% in the control to 47.1% and 32.2% after treatment with **Cu1** and **Cu2** respectively. In addition, increased activation of caspase-8/9 was observed from 2.8%/1.8% in the control to 21.1%/50.6% and 22.6%/40.0% after treatment with **Cu1** and **Cu2**, respectively (Fig S12). All these observations demonstrated that the copper complexes were potent in the activation of caspases. Therefore, **Cu1** and **Cu2** are excellent activators of all three caspases and can trigger apoptosis in A549 cells.

[Fig. 4]

[Fig. 5]

To determine the anticancer mechanism, we further analyzed the cell cycle of A549 cells after treatment with **Cu1** (1.5, 3.0 and 6.0 μM) and **Cu2** (3.0, 6.0, and 12.0 μM). The flow cytometry data exhibited an increase in % population of cells in the G1-phase of **Cu1** (45.7%, 56.5%, and 74.5%) and **Cu2** (48.3%, 56.4%, and 64.8%) compared with that in the control (G1: 38.9%) after treatment with three different concentrations (1.5, 3.0, 6.0 μM and 3.0, 6.0, 12 μM) of the copper complexes, which clearly showed the arrest of the G0/G1-phase in A549 cells by both the copper complexes. These results showed that **Cu1** and **Cu2** arrested the cell cycle at the G1-phase in A549 cells; thus, no replication of DNA occurred, and the cell cycle was blocked at the G1-phase (Figs. 6, S13, S14). In addition, the extent of cell cycle arrest by **Cu1** was greater than that by **Cu2**. Indeed, western blot results further indicated that the expression of cell cycle-related proteins, such as cyclin D, cyclin E, and cyclin A, as well as cyclin dependent kinases (CDK2 and CDK6) were down-regulated after treatment with the copper complexes for 24 h. However, the levels of p21, p27, and p53 were significantly upregulated. The decrease in the expression of cyclins and increase in the expression of cyclin dependent kinase inhibitors (CDKIs) confirmed cell cycle arrest at the G1-phase and induction of apoptosis. These observations are consistent with the flow cytometry results (Fig. S15).

[Fig. 6]

2.5.2. Activation of mitochondrial/ROS/ER-stress pathway

The mitochondria are considered an important cellular organelle in the induction of apoptosis. Therefore, targeting mitochondria is considered a new strategy for the discovery of novel anticancer drugs. The mitochondrial membrane potential is well-regulated and highly controlled [40]. Apoptotic pathways are activated when there is damage to the mitochondrial membrane

potential, which releases pro-apoptotic factors and ultimately leads to cell death [41]. To examine the effects of copper complexes, A549 cells were incubated with **Cu1** (1.5, 3.0, 6.0 μM) and **Cu2** (3.0, 6.0, 12.0 μM) for 24 h. A fluorescent dye JC-1 (5,5′,6,6′-tetrachloro-1,1′,3,3′-tetraethylbenzimi-dazolylcarbocyanine iodide) was used for analyzing mitochondrial membrane polarization using flow cytometry. A dose-dependent increase was observed in **Cu1-** and **Cu2**-treated cells from 1.36% cells in the control to 54.8% and 46.8%, respectively, at maximum concentration. These results indicate that apoptosis was induced by the copper complexes in A549 through mitochondrial-mediated pathways. The possibility of involvement of other pathways also existed (Figs. 7, S16, S17). Moreover, **Cu1** showed more effective damage on the membrane potential of mitochondria.

ROS is mainly produced in mitochondria, and the excessive production of ROS is harmful to mitochondria, disturbing its membrane potential and genetic stability and resulting in apoptotic cell death [42]. Therefore, we aimed to determine the ROS production in A495 cells after treatment with **Cu1** and **Cu2**. To this end, the A549 cells were treated with **Cu1** (3.0 μM, very close to the IC_{50} value) and **Cu2** (6.0 μM, very close to the IC_{50} value), for 24 h and analyzed using flow cytometry. As shown in Fig. 8A, we found that a high level of ROS was generated by the **Cu1** and **Cu2** complexes compared to that with the control. In addition, the density functional theory (DFT) calculation results show that the coordination geometrical structure and charge distribution of the two copper complexes are not much different, but they show a difference in the energy level of frontier molecular orbital due to the electron donating character of methoxy group. The energy level of the single-occupied molecular orbital (SOMO) of **Cu1** with two methoxy groups is slightly higher (–0.184 hartree) than **Cu2** with one methoxy groups (–0.187 hartree). Therefore, it may lead to a better activity in the generation of reactive

oxygen species for **Cu1** than **Cu2**. We further analyzed ROS-induced endoplasmic reticulum stress. To this end, A549 cells were treated with the copper complexes and analyzed based on the oxidation of H_2DCFDA (2′,7-dichlorodihydrofluorescein diacetate) to DCF (2′,7′-dichlorofluorescein) by ROS and (endoplasmic reticulum stress) ER-stress was analyzed using ER-Tracker Red. The results clearly showed colocalization, but with an increase in concentration, the ROS exhibited less colocalization and more diffusion with higher permeabilization of the endoplasmic reticulum membrane which led to the induction of ER-mediated apoptosis (Fig. 8B). We further confirmed the ER-stress pathway using western blot analysis. As shown in Fig. 9, **Cu1** and **Cu2** can induce the over production of CCAAT-enhancer-binding homologous proteins (CHOP) and the activation of Eukaryotic initiation factor 2 (eIF2α) and Protein kinase RNA-like endoplasmic reticulum kinase (PERK) in A549 cells. Together, these results confirmed the ER-stress mediated apoptosis by the copper complexes in A549 cells.

[Fig. 7]

[Fig. 8]

[Fig. 9]

2.5.3. Induction of autophagy by activating the MAPK signaling pathway

LC3 is a cytosolic protein (light chain-3 protein) linked with autophagy. This protein is conjugated with phosphatidylethanolamine in the cytosolic form to prepare the LC3-II complex which helps the induction of cell autophagy [43]. Another autophagic receptor protein SQSTM1/p62 (sequestosome1) interacts with LC3, which is continuously degraded during autophagy, and is associated with autophagy-dependent eradication of several substances [44]. Furthermore, an autophagy related Bcl-2-interacting protein (Beclin-1) is essential in the regulation of autophagy and apoptosis. Apoptosis and autophagy are interconnected by the

Beclin-1 caspase-mediated cleavage [45]. Interestingly, we found that treatment of A549 cells with **Cu1** and **Cu2** resulted in the upregulation of LC3-II and Beclin-1, whereas down-regulation of p62 and LC3-I (Fig. 10A). The results revealed the activation of autophagy as well as the link between autophagy and apoptosis [46]. To further confirm the autophagy pathway, western blot analysis of related proteins was performed. P38MAPK proteins are involved in the direction and regulation of cellular responses, autophagy, and apoptotic pathways [47]. The expression level of p38MAPKs was upregulated in A549 cells treated with **Cu1** and **Cu2**, which indicated that the p38MAPK pathway was activated and p38MAPK-mediated apoptosis occurred. In addition, cell survival proteins, such as protein kinase B also known as AKT (Activation of the phosphatidylinositol 3-kinase/protein kinase B) promote cell survival and inhibit apoptosis. Bcl-2 death associated (BAD) protein is phosphorylated by AKT, which is isolated as a Bcl-2/Bcl-xL complex, and inhibits proapoptotic capability. The targeting of AKT by the anticancer drugs results in tumor growth inhibition and apoptosis [48]. The western blot results showed the level of expression of AKT was downregulated. The results provide evidence of induction of apoptosis and autophagy, which are associated with AKT and p38MAPK signaling pathways, in A549 cells by **Cu1** and **Cu2** (Fig. 10B).

[Fig. 10]

2.5.4. Competitive binding studies

Comparatively less amount of copper was found in the nucleic fraction, during the investigation of cellular uptake and distribution of complexes in different parts of A549 cells. It implies that DNA may be act as a potential target. Therefore, ethidium bromide (EB) was used as a competitive intercalative probe for the investigation of binding abilities of **Cu1**, **Cu2** and cisplatin to the Calf Thymus-DNA (ct-DNA). When the EB-DNA system as [EB] / [DNA] = 1 : 10 ([EB] = 2 mM, [DNA] = 2 mM was excited by 350 nm light in the competitive binding

study, a characteristic strong emission was observed at 610 nm, depicted that the EB intercalated molecule has been significantly protected from the quenching caused by water in the DNA by the adjacent base pairs of the DNA. When the ratios of the concentration of [EB] / [DNA] / [**Cu1**] and [EB] / [DNA] / [**Cu2**] were increased from 1:10:1 to 1:10:10, a significant quenching in the characteristic emission of EB has been observed, as shown in Fig. 11. The K_{SV} constants were calculated by Stern-Volmer equation as 5.518×10^{3} for **Cu1** and 4.07×10^{4} for **Cu2**, respectively. It was found that both the metal complexes could moderately quench the fluorescence emission of EB, which strongly suggests that they could competitively interact with DNA via an intercalative binding mode at the similar binding sites of DNA with EB, whereas the cisplatin has no intercalative binding mode with DNA as shown (Fig. S18). The cisplatin covalently binds to the deoxyribonucleic acid (DNA) at the N-7 position of guanine (G) or adenine (A) sequences of GG and AG, to form an inter and intra-strand cross-linkages respectively [49].

[Fig. 11]

2.6. In vivo anticancer activity

The in vivo anticancer activity of **Cu1** and **Cu2** was investigated using a xenograft model of mice bearing A549 cells. Four groups of randomly divided mice were treated with vehicle (negative control), cisplatin (positive control), **Cu1,** and **Cu2**. The mice were treated intraperitoneally with low and high doses of **Cu1** and **Cu2** (7.5 and 15 mg/kg, respectively). Injection of the positive control with cisplatin (2 mg/kg) and negative control with 5% DMSO in saline was performed when the volume of the tumor reached 100–130 mm^3 (Figs. 12, 13). There was no obvious change observed in the body weight of **Cu1**-, **Cu2**-, and negative control-treated groups. A significant weight loss was observed in the cisplatin-treated group during the 15-day-

treatment (Figs. 12B, 13B). The tumor growth was inhibited by **Cu1** (21.1% and 41.3%) and **Cu2** (19.5% and 41.7%) to a higher extent than that with the control, but lower than that by cisplatin which was 57.5 % (Figs. 12C, 13C). These experiments showed that **Cu1** and **Cu2** exhibited a higher in vivo safety profile than cisplatin and effectively inhibited tumor growth.

[Fig. 12]

[Fig. 13]

3. Conclusion

Two new copper agents, **Cu1** and **Cu2,** displayed high selective cytotoxicity against human tumor cells by a multi-targeted anticancer mechanism. Importantly, the complexes exhibited less toxicity against human normal cells (HL-7702). A mechanistic study showed that the agents induced bimodal death through apoptosis and autophagy in A549 cells. **Cu1** and **Cu2** induced cytotoxicity via mitochondria-mediated apoptosis which initiated the caspase cascade and ROS generation that produced ER stress and the MAPK apoptotic pathway that collectively caused cell death. Furthermore, **Cu1** and **Cu2** regulated the pro-death autophagy proteins such as Beclin1, p62, LC3-1 and LC3-II and induced autophagy. Both **Cu1** and **Cu2** induced mitochondrial-mediated apoptosis and pro-death autophagy (Fig. 14). **Cu1** and **Cu2** interacted with ct-DNA via an intercalative binding mode. The slightly different biological behavior of **Cu1** and **Cu2** could be attributed to the position and number of the methoxy group. Experiments also showed that **Cu1** and **Cu2** effectively inhibited the tumor growth in a xenografted mouse model bearing A549 cells but exhibited lower in vivo toxicity than cisplatin. **Cu1** and **Cu2** could be developed as potential anticancer agents.

[Fig. 14]

4. Experimental methods

4.1. Materials

Chemical reagents were purchased from Alfa Aesar (Ward Hill, Massachusetts, USA), Sigma Aldrich (Saint Louis, Missouri, USA), and Xilong Scientific Co., Ltd. (China) and used as received without further purification. Dimethyl sulfoxide (DMSO) of analytical grade was used for the preparation of stock solutions of the copper complexes. The working solutions of different concentrations used for the various biological experiments were prepared by dilution of stock solution in PBS. Compounds of more than 97% purity were used for the pharmacological studies and spectroscopic and biological experiments. Kits used for performing different biological assays such as the MTT assay, cell cycle determination, detection of apoptosis, determination of mitochondrial membrane potential, ROS Detection Assay Kit, and Caspases Colorimetric Assay Kit were purchased from BD Biosciences (San Jose, CA, USA) and BioVision (Milpitas, California, USA). The primary and secondary antibodies were purchased from Abcam (Cambridge, MA, USA). The A549 xenograft mouse model was purchased from Beijing Biosciences Co., Ltd. (Beijing, China).

4.2. Instruments

Electrospray ionization mass spectrometry (ESI-MS) spectra were obtained on a Bruker HCT mass spectrometer. A Bruker AV-500 NMR spectrometer was used for obtaining (Nuclear magnetic resonance spectroscopy) NMR spectra. Crystallographic data were recorded on a Bruker smart APEX II machine. UV absorption spectra were recorded on a TU-1901 UV-spectrometer. Elite P230II (Dalian, China) was used for HPLC analysis. A Tecan Microplate reader M1000 T (Shanghai, China) was used for performing the MTT assay. A FACS Arial II flow cytometer BD Biosciences (San Jose, CA, USA) was used for performing the flow

cytometry analysis. The ECL western blotting system was used for the detection and confirmation of protein expressions.

4.3. Synthesis of ligands (L^1 and L^2)

Both ligands and intermediate products were synthesized according to reported procedure [34]. The NMR data, including ^{1}H-NMR and ^{13}C-NMR, and ESI-MS are given in supporting information.

4.3.1. N-(4-methoxyphenethyl)-2-nitrobenzamide and N-(3,4-dimethoxyphenethyl)-2-nitrobenzamide (1a-b) general procedure A: Nitrobenzoic acid (0.1 mol) and thionyl chloride were treated in dry dichloromethane (CH_2Cl_2). The resulting mixture was stirred for 12 h at 70 °C. The excess thionyl chloride was discarded under reduced pressure and the resulting solution was dissolved in benzene. This solution was added dropwise to the corresponding 0.1 mol amines, [(2-(3,4-dimethoxyphenyl)ethan-1-amine) and 2-(4-methoxyphenyl)ethan-1-amine], in dry benzene. The reaction mixture was stirred continuously for 12–16 h at 25 °C. This mixture was washed with 500 mL water, then separated and the organic layer collected. The product was recrystallized in *n*-hexane/methanol. ESI-MS: *m/z* (1a) = 329.11 $[M - H]^-$, (1b) = 301.12 $[M + H]^+$. (Figs. S19, S20).

4.3.2. 6,7-Dimethoxy-1-(2-nitrophenyl)-3,4-dihydroisoquinoline and 6-methoxy-1-(2-nitrophenyl)-3,4-dihydroisoquinoline (2a-b) general procedure B: To a stirred solution of 1(a) 200 mmol and 1(b) 200 mmol dissolved in acetonitrile (800 mL), $POCl_3$ (150 mL) was added and continuously stirred for 1 h at room temperature. Then, the mixture was refluxed for 10 h and monitored by thin layer chromatography (TLC), until completion of the reaction and all the starting material was consumed. Water (500 mL) and dichloromethane (500 mL) were added after the removal of the solvent by vacuum. The pH of the aqueous phase was adjusted to 10 by

the addition of 10 N NaOH. The organic phase was washed with an aqueous solution of $NaHCO_3$ (500 mL), dried with $MgSO_4$, and concentrated with reduced pressure. The target product was precipitated after sonication with methanol. ESI-MS: *m/z* (2a) = 313.11 $[M + H]^+$, (2b) = 283.10 $[M + H]^+$. (Figs. S21, S22).

4.3.3. 6,7-Dimethoxy-1-(2-nitrophenyl)isoquinoline and 6-methoxy-1-(2-nitrophenyl)isoquinoline (3a-b) general procedure C: Activated MnO_2 (0.6 g) was added to the refluxed solution of (2a) 10 mmol and (2b) 10 mmol in dry $CHCl_3$ once every 30–40 min, and the reaction was completed within 30 h. The reaction was monitored by TLC. On completion of the reaction, the hot mixture was filtered, and the filter cake was washed with dichloromethane (500 mL). The black particles of MnO_2 were removed through filtration on Celite, and the filtrate was dried using $MgSO_4$. The target product was obtained after recrystallization in methanol. ESI-MS: *m/z* (3a) = 311.09 $[M + H]^+$, (3b) = 281.08 $[M + H]^+$. (Figs. S23, S24).

4.3.4. 2-(6,7-Dimethoxyisoquinolin-1-yl) aniline (L^1) and 2-(6-methoxyisoquinolin-1-yl) aniline (L^2) general procedure D: $SnCl_2.2H_2O$ (26.4 mmol) was added to the stirred solution of 8 mmol each of (3a) and (3b) dissolved in dry ethyl acetate (150 mL) and refluxed for 24 h. The reaction was monitored by TLC. After completion, water (30 mL) and 10 N NaOH (5 mL) were added. The resulting solution was mixed with $NaHCO_3$ (100 mL), extracted with ethyl acetate (150 mL), dried using $MgSO_4$, and the solvent evaporated. The target compound was obtained after recrystallization with ethyl acetate/*n*-hexane.

4.3.5. L^1: ^{1}H-NMR (500 MHz, $(CD_3)_2SO$) δ 8.43 (d, *J* = 4.6 Hz, 1H), 7.68 (d, *J* = 4.6 Hz, 1H), 7.44 (s, 1H), 7.22 (m, 2H), 7.18 (s, 1H), 6.91 (d, *J* = 6.3 Hz, 1H), 6.75 (td, *J* = 0.9, 6.0 Hz, 1H), 5.11 (s, 2H), 3.98 (s, 3H), 3.75 (s, 3H). ^{13}C-NMR (100 MHz, $(CD_3)_2SO$) δ 157.1, 157.0, 152.9,

150.1, 146.9, 141.1, 131.2, 129.5, 123.3, 122.7, 119.0, 116.4, 116.2, 105.9, 105.5, 56.2, 55.6. ESI-MS: m/z = 281.12 $[M + H]^+$. (Figs. S25–S27).

4.3.6. L^2: ^{1}H-NMR (500 MHz, $(CD_3)_2SO$) δ 8.50 (d, *J* = 4.7 Hz, 1H), 7.77 (m, 3H), 7.44 (d, *J* = 2.1 Hz, 1H), 7.26 (dd, *J* = 2.1, 8.0 Hz, 1H), 7.22 (m, 1H), 7.12 (dd, *J* = 1.1, 6.2 Hz, 1H), 6.74 (m, 1H), 5.09 (s, 2H), 3.96 (s, 3H). ^{13}C-NMR (100 MHz, $(CD_3)_2SO$) δ 160.6, 159.1, 146.9, 142.9, 139.2, 131.3, 129.6, 123.1, 122.6, 120.3, 119.5, 116.2, 116.1, 108.1, 105.4, 56.0. ESI-MS: m/z = 251.11 $[M + H]^+$. (Figs. S28–S30).

4.4. Formation of copper complexes

Cu1 and **Cu2** complexes were prepared in a Pyrex glass tube. Briefly, the copper salt, ligands, and solvent were placed in a glass tube and chilled with liquid nitrogen. The ice-chilled tube was evacuated and sealed using a torch flame and placed at 80 ºC for 72 h. Block crystals were formed by slow cooling to room temperature. Elemental analysis IR and ESI-MS were performed, and the acquired data are presented in Supporting Information.

4.4.1. Cu1: (Yield 60–70%), Anal. Calc. (%) for $C_{17}H_{16}Cl_2CuN_2O_2$: C, 49.23; H, 3.89; N, 6.75; O, 7.71. Found (%): C, 49.35; H, 3.98; N, 6.80; O, 7.81. IR (KBr) ν_{max} cm^{-1}: 3271 (N–H stretching), 1610 (aromatic ring vibration), 1077–1265 (C–O), 200–300 (Cu–Cl), 300–600 very weak (Cu–N). ESI-MS *m/z*: 412.9. (Figs. S31, S32).

4.4.2. Cu2: (Yield 60–70 %), Anal. Calc. (%) for $C_{16}H_{14}Cl_2CuN_2O$: C, 49.95; H, 3.67; N, 7.28; O, 4.16. Found (%): C, 50.08; H, 3.92; N, 7.40; O, 4.45. IR (KBr) ν_{max} cm^{-1}: 3251 (N–H stretching), 1618 (δ (NH_2 bending)), 1473 (C–N), 1265 (C–O), 200–300 (Cu–Cl). ESI-MS *m/z*: 382.9. (Figs. S33, S34).

4.5. In vitro experiments

4.5.1 Culturing of cells

Cells, including T-24, MGC-803, HeLa, A549, SKOV-3, and MDA-MB216 and human normal liver cells HL-7702 were purchased from the Shanghai Cell Bank of the Chinese Academy of Sciences. They were grown at a constant temperature of 37 °C and under humidified air of 5% CO_2 with Dulbecco's modified eagle medium containing 5% fetal bovine serum. Dimethyl sulfoxide was used for the dissolution of copper complexes. The stock solution was 2 mM, and the working solution was prepared by dilution with PBS to the required concentration. The cisplatin stock solution was prepared by dissolving 24 mg powder in 10 mL of 0.9% saline, and the solution was kept at 4 ℃. On each day of the experiment, a quality control sample was freshly prepared.

4.5.2. MTT assay

96-Well plates were used for this assay. The cells were seeded at a density of 6×10^3/180 µL in each well for 24 h. To prepare the required concentration, 20 µL medium having different concentrations of each compound was added to the wells and the cells were incubated for 48 h. To the control well, 0.5% DMSO was added. Subsequently, 10 µL MTT (5 mg/mL) was added and incubated for another 6 h under the same conditions. The medium was discarded, and the crystalized form of formazan was dissolved in 100 µL DMSO. A microplate reader with the double wavelength of 490/630 nm was used for measuring absorption. This assay was independently performed thrice in triplicate. The Bliss method (n = 5) was used for the calculation of IC_{50} values.

4.5.3. Morphological analysis of cells

Cells were cultivated at a suitable temperature (37 °C) and under CO_2 (5%). After attachment, the cells were exposed to **Cu1** and **Cu2** and incubated for 24 h in the same environment. Cell morphology was examined under a bright-field microscope.

4.5.4. Cell cycle analysis

Cells at the density of 5–7 × 10^6 were cultured in a 50 mm plate for 24 h. The cells were incubated with various concentrations of **Cu1**, **Cu2**, and cisplatin for 24 h. After 24-h treatment, the cells were fixed with 75% prechilled ethanol and placed for one night at -20 °C. Cells were washed with PBS and resuspended. The cells were incubated with PBS containing RNAs (100 µg/mL) and propidium iodide (PI) (50 µg/mL) for 30 min in the dark. BD FACS Calibur Flow cytometer was used for analysis. Mod FIT LT version 3.3 (Variety Software House) was used for the calculation of cell cycle distribution.

4.5.5. Apoptosis analysis

A 6-well plate was used for overnight culturing of cells at a density of 2 × 10^6 at 37 °C. The cells were treated with the copper complexes for 24 h. After incubation, the cells were collected and washed with PBS. An apoptosis detection kit was used according to the manufacturer's instructions. A BD FACS flow cytometer was used for analysis.

4.5.6. ROS generation

Cells were cultured at a density of 1 × 10^5 in a 6-well plate for 24 h at 37 °C. The cells were treated with the copper complexes for 24 h. After treatment, the cells were collected and washed to remove the medium and then incubated with 2′,7′-Dichlorodihydrofluorescein diacetate (DCFH-DA) for 25 min in the dark. The cells were washed again with 1 mL of PBS. A BD FACS flow cytometer was used for the detection of generated ROS and measurement of 2′, 7′ – dichlorofluorescein (DCF) fluorescence. DCFH-DA (non-fluorescent) was converted to DCFH by the enzymatic action of esterase and as DCFH is not very stable it was quickly converted to DCF (a fluorescent compound). The fluorescence intensity of DCF depends on the production of ROS.

4.5.7. Mitochondrial membrane potential

The JC-1 staining kit was used for the determination of mitochondrial membrane potential. A549 cells were cultured at a density of 1×10^5 in a 6-well plate for 24 h at 37 °C. The cells were treated with different concentrations of copper complexes for 24 h. After treatment, the cells were harvested and washed with PBS to remove the medium and incubated with JC-1 for 25 min in the dark. To prepare the sample for BD FACS flow cytometer, 0.5 mL PBS was added to the samples to determine the mitochondrial membrane potential.

4.5.8. Determination of activated caspases 3, 8, and 9

Cells were placed in a 6-well plate for 24 h at a density of 1×10^6 at 37 °C. After 24-h treatment with the copper complexes the cells were washed with PBS to remove the medium and incubated with 1 µL of caspase 3, 8, and 9 inhibitors, fluorescein isothiocyanate-Asp-Glu-Val-Asp-fluoromethyl ketone (FITC-D(OMe)-E(OMe)-VD(OMe)-FMK) for 1 h in the dark. The BD FACS flow cytometer was used for the determination of caspases activation in copper complexes-treated cells compared with that in the negative control.

4.5.9. ROS visualization of endoplasmic reticulum

Cells were placed on coverslips coated with poly-L-lysin in a 6-well plate for 24 h at the density of 2×10^6 cells in each well. The cells were exposed to copper complexes for 7 h, and then, cells were washed with prewarmed PBS. The cells were then incubated with 25 mM H_2DCFDA (2′,7-dichlorodihydrofluorescein diacetate) for 25 min. After addition of ER-Tracker Red (1 mM), the cells were washed with PBS and mounted cells were visualized using confocal microscopy. Zeiss FLUOVIEW was used for processing images acquired using a 20× objective lens.

4.5.10. Western blotting analysis

Cells were placed in a 100 mm culture plate for 24 h. When the cells were ready for treatment, the copper complexes were added at various concentrations and incubated for more than 24 h at 37 °C. After 24 h, the cells were harvested, washed with PBS, and lysed with lysis buffer (149 µL) and 1 µL phenylmethylsulfonyl fluoride (PMSF). Total proteins were extracted by centrifugation (15000G g) at 4 °C for 20 min before the samples were put on ice for 40 min. A mixture of purified proteins (50 µg) and an equal volume of electrophoresis sample buffer was prepared and boiled for 5–8 min including the controls. The samples were run on 12% SDS-PAGE (sodium dodecyl sulfate-polyacrylamide gel electrophoreses) and then transferred to a PVDF (polyvinylidene fluoride) layer. The membrane was blocked using TBS buffer (tris-buffered saline) of 5% BSA for 2 h, after the complete transfer of proteins from the gel to the membrane. The PVDF was washed with PBS and incubated overnight at 4 °C with suitable primary antibodies. After incubation with primary antibodies, the membrane was incubated with secondary antibodies for 2 h at room temperature. The membrane was washed with PBS before and after incubation with antibodies. Immunoreactive signals were detected using a chemo-luminance kit according to the procedure described by the manufacturer.

4.5.11. In vivo experiments

BALB/c nude mice (male, aged 30–40 days, 18–22 g) were provided by the Guangxi Medical University Laboratory Animal Centre (Guanxi, China). The mice were placed in individually ventilated cages with a humidified atmosphere of 45–50% at 25–30 °C with a constant duration of light and dark (12 h light, 12 h dark). For the development of tumor, A549 cells at a density of 5×10^6 were injected into the right flank of mice. The mice were sacrificed when the xenograft tumor reached 1000 mm^3. The tumor tissue was cut into pieces of 1.6 mm^3 and then translocated to the nude male mice. When the tumor tissue reached 100–160 mm^3, all the mice were divided

randomly into groups including solvent controls and complexes-treated groups. Cisplatin was used as a positive control and was administrated at 2 mg/kg per two days. The negative control comprised treatment with 5% DMSO v/v per saline. **Cu1** and **Cu2** were administered in low and high doses of various concentrations (7.5 and 15 mg/kg, respectively). For the systemic safety of complexes, the body weight was taken as a parameter and was recorded every three days. The tumor size was also recorded at three-day intervals. The mice were sacrificed after 15 days and the tumor weight was recorded. The formula $V = L \times W^2/2$ was used for the calculation of tumor volume (V) using the measured width (W) and length (L) of the tumor. The rate of tumor growth was determined using the formula $(L\text{-}TW_t/TW_c) \times 100$, where TWt represents the complex-treated mice and TW_c represents the vehicle-treated mice [50-52].

4.5.12. Computational details for DFT

All calculations were performed using Gaussian 16 program Rev. A.03 [53]. Geometry optimizations were carried out with M06-L/def2-SVP level of theory [54,55]. Frequency analysis calculations were performed to characterize the structures to be the minima (no imaginary frequency). The 3D optimized structure figures in this paper were displayed by IBOview visualization program [56]. Additional computational information and the Cartesian coordinates (xyz) of the optimized structures and figure are given in the supporting information (Fig. S35).

4.5.13. Fluorescence emission titration

A solution of DNA (2 mM) and EB (2 mM) with 10:1 ([DNA] / [EB]) was prepared for competitive binding studies. Using Stern-Volmer equation ($I_0 / I = 1 + Ksv \times [Q]$) the quenching constant were calculated of the tested compounds. In this equation the I_0 and I represented the highest emission intensities of the EB-DNA system with and without the presence of quencher. *Ksv* represented the Stern-Volmer quenching constant, that is obtained by the linear fitting of the

plot I_0 / I against [Q], and to determine the quenching ability of small molecules on EB indicated as a DNA intercalative probe.

4.6. Statistical analysis

The experiments were conducted in 3–6 replicates. The Student's *t*-test was used to measure significant differences and the results are reported as the mean ± SD. The difference was considered statistically significant when the *p*-value was less than 0.05.

Abbreviations

DMEM	Dulbecco's modified eagle medium
FBS	Fetal bovine serum
MMP	Mitochondrial membrane potential
Bax	Bcl-2-associated X protein
Bak	Bcl-2 antagonist / killer protein
Bcl-2	B-cell lymphoma 2
Bcl-xl	B-cell leukemia xl
ROS	Reactive oxygen species
MAPK	Mitogen-activated protein kinases
LC3	Light chain3 proteins
PERK	Protein kinase RNA-like endoplasmic reticulum kinase
eIF2α	Eukaryotic initiation factor-2
CHOP	CCAAT-enhancer-binding homologous proteins
SQSTM1	Sequestosome1
MTT	Microculture tetrazolium assay

IC_{50}	The half maximal inhibitory concentration
PI	Propidium iodide
PBS	Phosphate buffer saline
DCFH-DA	Dichloro-dihydro-fluorescein diacetate
ER-stress	Endoplasmic reticulum stress
SDS-PAGE	Sodium dodecyl sulfate (SDS) polyacrylamide gel electrophoresis
MDA-MB216	Invasive ductal carcinoma
CDKs	Cyclin dependent kinases
Caspases	Cysteine-dependent aspartate-directed proteases

Acknowledgment

This work was supported by the National Natural Science Foundation of China (Grant 21431001), IRT_16R15, and the Natural Science Foundation of Guangxi Province of China (Grants: 2016GXNSFGA380005 and AD17129007), and the "BAGUI Scholar" program of the Guangxi Province of China.

Supporting Information

Vendor codes for **Cu1** and **Cu 2** crystal data, HPLC, ESI-MS, and IR data. The supplementary crystallographic data of this paper can be seen under the CCDC No. 19811393, 19811396.

Author Contributions

Noor Shad Gul[#] and Taj-Malook Khan[#] contributed equally to this work denoted by a superscript (#).

References

Journal Pre-proof

[1] S. Rafique, M. Idrees, A. Nasim, H. Akbar, A. Athar, Biotechnol. Mol. Biol. Rev. 5 (2010) 38–45.

[2] L. Kelland, Nat. Rev. Cancer 7 (2007) 573–584.

[3] L. Amable, Pharmacol. Res. 106 (2016) 27–36.

[4] S.M. Dencic, J. Poljarevic, A.M. Isakovic, T. Sabo, I. Markovic, V. Trajkovic, Curr. Med. Chem. 27 (2020) 380–410.

[5] S. Ghosh, Bioorg. Chem. 88 (2019) 203–208.

[6] R. Oun, Y.E. Moussa, N.J. Wheat, Dalton Trans. 47 (2018) 6645–6653.

[7] D.E. Gerber, Am. Fam. Physician. 77 (2008) 311–319.

[8] D. Hanahan, R.A. Weinberg, Cell 144 (2011) 646–674.

[9] W. Zheng, Y. Zhao, Q. Luo, Y. Zhang, K. Wu, F. Wang, Curr. Topic Med. Chem. 17 (2017) 3084–3098.

[10] S. Banerjee, Y. Li, Z. Wang, F. H. Sarkar, Cancer Lett. 269 (2008) 226–242.

[11] U.N. dagi, N. M. hlongo, M. E. Soliman, Drug Des. Devel. Ther. 11 (2017) 599–616.

[12] C.R. Kowol, P. Heffeter, W. Miklos, L. Gille, R. Trondl, L. Cappellacci, W. Berger, B.K. Keppler, J. Biol. Inorg. Chem. 17 (2012) 409–423.

[13] A.S. Potapov, E.A. Nudnova, G.A. Domina, L.N. Kirpotina, M.T. Quinn, A.I. Khlebnikov, I.A. Schepetkin, Dalton Trans. 23 (2009) 4488–4498.

[14] I. Schepetkin, A. Potapov, A. Khlebnikov, E. Korotkova, A. Lukina, G. Malovichko, L. Kirpotina, M.T. Quinn, J. Biol. Inorg. Chem. 11 (2006) 499–513.

[15] J.A. Ahsan, A.A. Khan, Z. Ali, R. Haider, M.S. Yar, Eur. J. Med. Chem. 125 (2017) 143–189.

Journal Pre-proof

[16] S.S. Gu, P. Yu, J.N. Hu, Y. Liu, Z.W. Li, Y. Qian. Y. Wang, Y. Gou, F. Yang, Eur. J. Med. Chem. 164 (2019) 654–664.

[17] M. Wehbe, A.W.Y. Leung, M.J. Abrams, C. Orvig, M.B. Bally, Dalton Trans. 46 (2017) 10758–10773.

[18] F.G. Parsa, M.A.H. Feizi, R.S. Alizadeh, S.A.H Yazdi, M. Mahdavi, J. Biol. Inorg. Chem. 25 (2020) 383–394.

[19] S. Monro, K.L. Colón, H. Yin, J. Roque, Chem. Rev. 119 (2019) 797–828.

[20] A. Kellett, Z. Molphy, C. Slator, V. McKee, N.P. Farrell, Chem. Soc. Rev. 48 (2019) 971–988.

[21] D. Colangelo, A.L. Ghiglia, I. Viano, G. Cavigiolio, D. Osella, Biometals 16 (2003) 553–560.

[22] J. Malina, N.P. Farrell, V. Brabec, Angew. Chem. Int. Ed. 57 (2018) 8535 –8539.

[23] C. Santini, M. Pellei, V. Gandin, M. Porchia, F. Tisato, C. Marzano, Chem. Rev. 114 (2013) 815–862.

[24] D.B. Lovejoy, P.J. Jansson, U.T. Brunk, J. Wong, P. Ponka, D.R. Richardson, Cancer Res. 71 (2011) 5871–5880.

[25] F. Tisato, C. Marzano, M. Porchia, M. Pellei, C. Santini, Med. Res. Rev. 30 (2010) 708–749.

[26] I. R. Canelon, P. J. Sadler, Inorg. Chem. 52 (2013) 12276–12291.

[27] N.S. Moorthy, N.M. Cerqueira, M.J. Ramos, P.A. Fernandes, Anticancer Drug Discov. 8 (2013) 168–182.

[28] A. Bergamo, G. Sava, Chem. Soc. Rev. 44 (2015) 8818–8835.

Journal Pre-proof

[29] M. Saxena, J. Saxena, R. Nema, D. Singh, A. Gupta, J. Pharmacogn. Phytochemistry 1 (2013) 168−182.

[30] M. Ferraroni, C. Bazzicalupi, A.R. Bilia, P. Gratteri, Chem. Commun. 47 (2011) 4917−4919.

[31] K.B. Huang, Z.F. Chen, Y.C. Liu, M. Wang, J.H. Wei, X.L. Xie, J.L. Zhang, K. Hu, H. Liang, Eur. J. Med. Chem. 70 (2013) 640−648.

[32] T.M. Khan, N.S. Gul, X. Lu, J. H. Wei, Y.C. Liu, H. Sun, H. Liang, C. Orvig, Z.F. Chen, Eur. J. Med. Chem. 163 (2019) 333−343.

[33] T. M. Khan, N. S. Gul, X. Lu, R. Kumar, M. I. Choudhary, H. Liang, Z. F. Chen, Dalton Trans. 48 (2019) 11469−11479.

[34] N. Sotomayor, E. Domínguez, E. Lete, J. Org. Chem. 61 (1996) 4062−4072.

[35] F.V. Nussbaum, B. Miller, S. Wild, K.S. Hilger, S. Schumann, H. Zorbas, W. Beck, W. Stiglich, J. Med. Chem. 42 (1999) 3478- 3485.

[36] Y.P. Ho, K.K. To, S.C. A. Yeung, X. Wang, G. Lin, X. Han, J. Med. Chem. 44 (2001) 2065−2068.

[37] Z.Q. Deng, P. Gao, L.L. Yu, B. Ma, Y.Y. You, L. Chan, C. Mei, T.F. Chen, Biomaterials 129 (2017) 111−126.

[38] R. Gerl, D.L. Vaux, 26 (2005) 263−270.

[39] L.H. Aung, R. Li, B.S. Prabhakar, A.V. Maker, P. Li, Oncotarget 8 (2017) 56582−56597.

[40] J. Armstrong, Br. J. Pharmacol. 151 (2007) 1154−1165.

[41] J. Chipuk, L.B. Hayes, D. Green, Cell Deat. Differ. 13 (2006) 1396−1402.

Journal Pre-proof

[42] P. Nagakannan, P. Tabeshmehr, E. Eftekharpour, Free Radical Biol. Med. https://doi.org/10.1016/j.freeradbiomed.2020.04.001.

[43] I. Tanida, T. Ueno, E. Kominami, Int. J. Biochem. Cell Biol. 36 (2004) 2503–2518.

[44] S. Pankiv, T.H. Clausen, T. Lamark, A. Brech, J. A. Bruun, H. Outzen, A. Øvervatn, G. Bjørkøy, T. Johansen, J. Biol. Chem. 282 (2007) 24131–24145.

[45] S. Pattingre, A. Tassa, X. Qu, R. Garuti, X.H. Liang, N. Mizushima, M. Packer, M.D. Schneider, B. Levine, Cell 122 (2005) 927–939.

[46] W.W. Li, J.Y. Yu, H.L. Xu, J.K. Bao, Biochem. Biophys. Res. Commun. 414 (2011) 282–286.

[47] X. Sui, N. Kong, L. Ye, W. Han, J. Zhou, Q. Zhang, C. He, H. Pan, Cancer Lett. 344 (2014) 174–179.

[48] M.E. Hardie, H.W. Kava, V. Murray, Curr. Pharm. Des. 22 (2016) 6645–6664.

[49] G. Song, G. Ouyang, S. Bao, J. Cell Mol. Med. 9 (2005) 59–71.

[50] H.Y. Lee, A. C. Tsai, M.C. Chen, P.J. Shen, Y.C. Cheng, C.C. Kuo, S.L. Pan, Y.M. Liu, J.F. Liu, T.K. Yeh, J. Med. Chem. 57 (2014) 4009–4022.

[51] P.H. Thaker, J. Y. Han, A.A. Kamat, J.M. Arevalo, R. Takahashi, C. Lu, N.B. Jennings, G.A. Pena, J.A. Bankson, M. Ravoori, Nat. Med. 12 (2006) 939–944.

[52] A. Ventura, D.G. Kirsch, M.E. McLaughlin, D.A. Tuveson, J. Grimm, L. Lintault, J. Newman, E.E. Reczek, R. Weissleder, T. Jacks, Nature 445 (2007) 661–665.

[53] M.J. Frisch, G.W. Trucks, H.B. Schlegel, G.E. Scuseria, M.A Robb., J.R. Cheeseman, G. Scalmani, V. Barone, G.A Peterson, H. Nakatsuji, X. Li, M. Caricato, Gaussian. 16 Rev. A.03. 2016.

[54] Y. Zhao, D.G. Truhlar, Accounts Chem. Res. 41 (2008) 157-167.

[55] F. Weigend, R. Ahlrichs, Phys. Chem. Chem. Phys. 7 (2005) 3297-3305.

[56] G. Knizia, J.E.M.N. Klein, Angew. Chem. Int. Ed. 54 (2015) 5518-5522.

Figure Legends

Fig. 1. Chemical structures of **Cu1** and **Cu2**.

Fig. 2. Crystal structures of **Cu1** and **Cu2**

Fig. 3. Cellular uptake and distribution of copper complexes in A549 cells as determined by inductively coupled plasma mass spectrometry (ICP-MS). DMSO was used as the control. A549 cells were treated with **Cu1** (3 μM) and **Cu2** (6 μM) for 20 h at 37 °C. Mean ± SD $*p < 0.05$, $**p < 0.01$ measured using ANOVA.

Fig. 4. Flow cytometric analysis of **Cu1** and **Cu2** in the induction of apoptosis of A549 cells using the fluorescence activated cell sorting (FACS) method with Annexin V and propidium iodide (PI) staining.

Fig. 5. Flow cytometric analysis of activated caspase-3, caspase-8, and caspase-9 caused by **Cu1** and **Cu2** and negative control (DMSO). One representative experiment is presented.

Fig. 6. Measurement of cell cycle arrest in A549 cells by **Cu1** and **Cu2**.

Fig. 7. Damage of mitochondrial membrane potential was measured using flow cytometry after 24-h treatment with **Cu1** and **Cu2**.

Fig. 8. (A) Measurement and graphical representation of reactive oxygen species (ROS) generation after treatment with **Cu1** and **Cu2** compared with negative (DMSO) control using flow cytometric analysis. Mean ± SD $*p < 0.05$, $**p < 0.01$ determined using ANOVA. (B)

Confocal micrograph of ROS generation in cells using DCFH (ROS indicator, green) and analysis of the endoplasmic reticulum sulfonylurea receptors using ER-Tracker Red (red).

Fig. 9. Western blot analysis of CHOP, PERK, and eIF2α. *$p < 0.05$ and **$p < 0.01$ determined using ANOVA.

Fig. 10. (A) Western blotting analysis of SQTM1, Beclin 1, and LC3-I and -II, and band intensity measured using Image J. Results of three independent experiments are shown. Mean ± SD *$p < 0.05$, **$p < 0.01$ determined using ANOVA. (B) MAPK pathways proteins, analysis of AKT and p38 by western blotting and quantification of bands using Image J (triplicate). *$p < 0.05$ and **$p < 0.01$ determined using ANOVA.

Fig. 11. Fluorescence emission spectra of EB bound with ct-DNA in the absence (dashed line ----) and presence (solid lines —) of Cu1 (2 mM) and Cu2 (2 mM) as competitive agent with increasing [EB] / [DNA] / [Cu1 or Cu2] ratios in the range of 1:10:1 to 1:10:10.

Fig. 12. In vivo anticancer activity of **Cu1** in xenografted mouse bearing A549 cells. (A) Effect of **Cu1** (7.5 and 15 mg/kg) on tumor growth compared with that of cisplatin (2 mg/kg) and negative control (5% DMSO in saline, v/v). The growth of the tumor was measured and calculated as mean ± SD of tumor volume (mm^3) and represented as the relative rate of tumor increment (%TC). (B) Comparative measure of tumor weight between treatments after sacrifice of mice. Mean ± SD with *$p < 0.05$, *$p < 0.01$, and ***$p < 0.001$ determined using ANOVA. (C) Body weight is recorded and displayed as % change from the initial weight. (D) Photograph representing the negative control, **Cu1-** and cisplatin-treated groups.

Fig. 13. In vivo antitumor activity of **Cu2** on the xenografted mouse model bearing A549 cells. (A) Effect of **Cu2** (7.5 and 15 mg/kg) on tumor growth in comparison with that in the negative control (5% DMSO in saline, v/v) and positive control (2 mg/kg cisplatin). The tumor volume

was calculated in mm^3 and is represented as the relative rate of tumor increment (%TC). (B) After sacrifice of mice, the weight of the tumor was compared with the initial weight taken as the standard. Mean ± SD with $*p < 0.05$, $*p < 0.01$, and $***p < 0.001$ determined using ANOVA. (C) Bodyweight is recorded and displayed as % change from the initial weight. (D) Photograph of the control, cisplatin-, and **Cu2-**treated groups.

Fig. 14. Proposed mechanism of **Cu1** and **Cu2** induced mitochondrial-mediated apoptosis and pro-death autophagy.

Journal Pre-proof

Table 1. IC_{50} values (μM) of copper complexes on seven tumor cell lines after 48 h.

Compounds	MGC803	T-24	SKOV-3	HeLa	A549	MDA-MB216	HL-7702
Cu1	21.3±0.5	18.2±0.8	15.1±0.7	10.1±0.4	3.1±0.3	11.6±0.4	35.1±0.4
Cu2	36.2±0.2	21.3±0.5	26.2±0.5	12.5±0.3	6.4±0.5	18.7±0.6	42.2±0.1
$CuCl_2.2H_2O$	55.1±0.5	60.1±0.6	45.1±0.4	41.4±0.2	33.1±0.5	29.3±0.5	51.8±0.4
L^1	60.3±0.9	67.1±0.4	50.4±0.5	59.3±0.4	57.0±0.3	49.1±0.3	57.1±0.3
L^2	75.5±0.3	92.3±0.8	69.4±0.5	84.1±0.5	60.1±0.2	73.4±0.2	69.7±0.2
Cisplatin	19.6±0.1	27.3±0.3	24.5±0.6	22.1±0.8	20.7±0.8	21.02±0.4	22.1±0.3

Cu1 (copper complex **1**), **Cu2** (copper complex **2**), L^1 (ligand **1**), L^2 (ligand **2**).

Journal Pre-proof

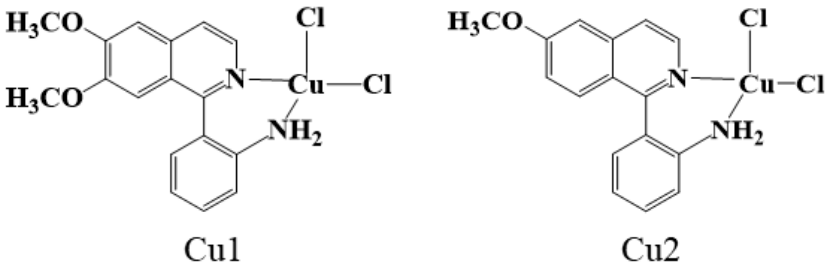

Fig 1.

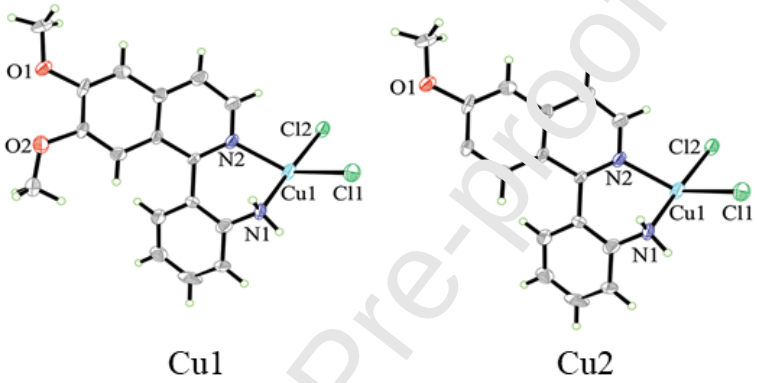

Fig. 2

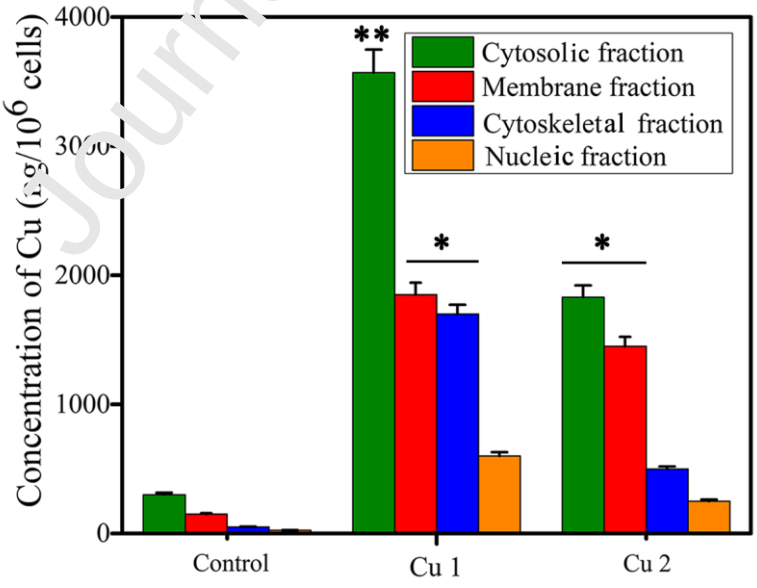

Fig. 3

Journal Pre-proof

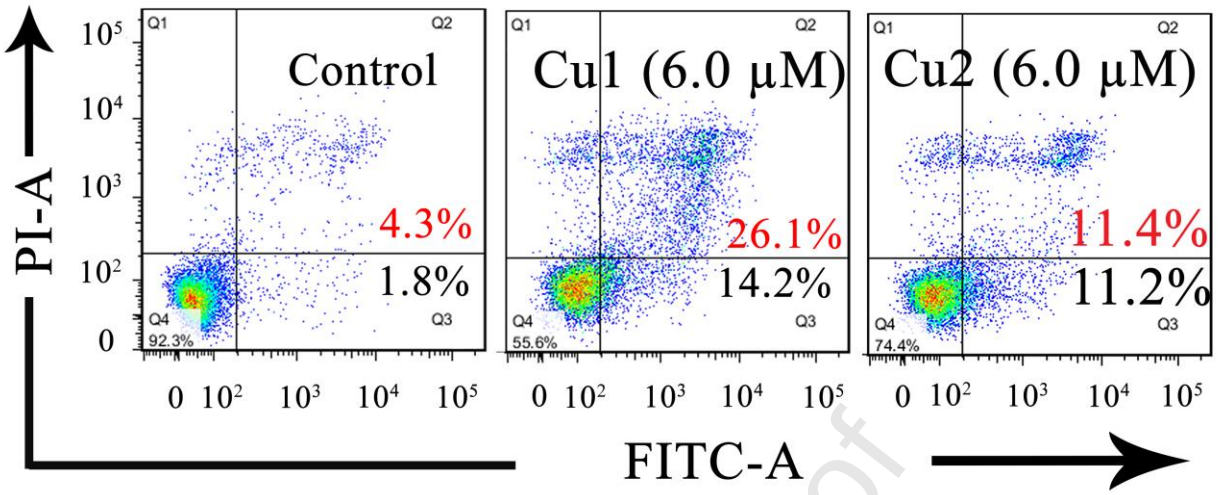

Fig. 4

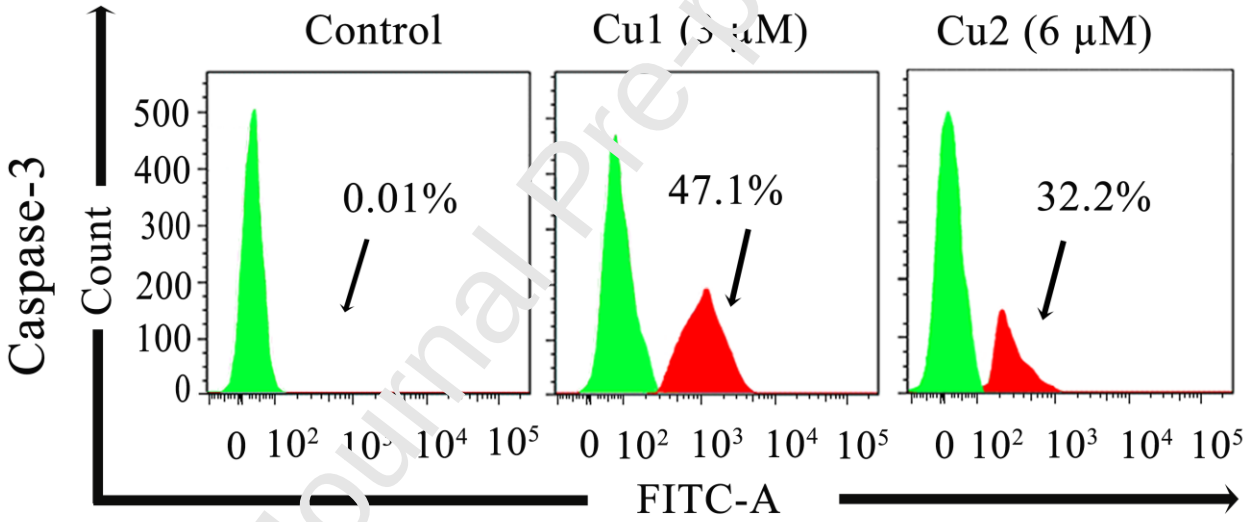

Fig. 5

Journal Pre-proof

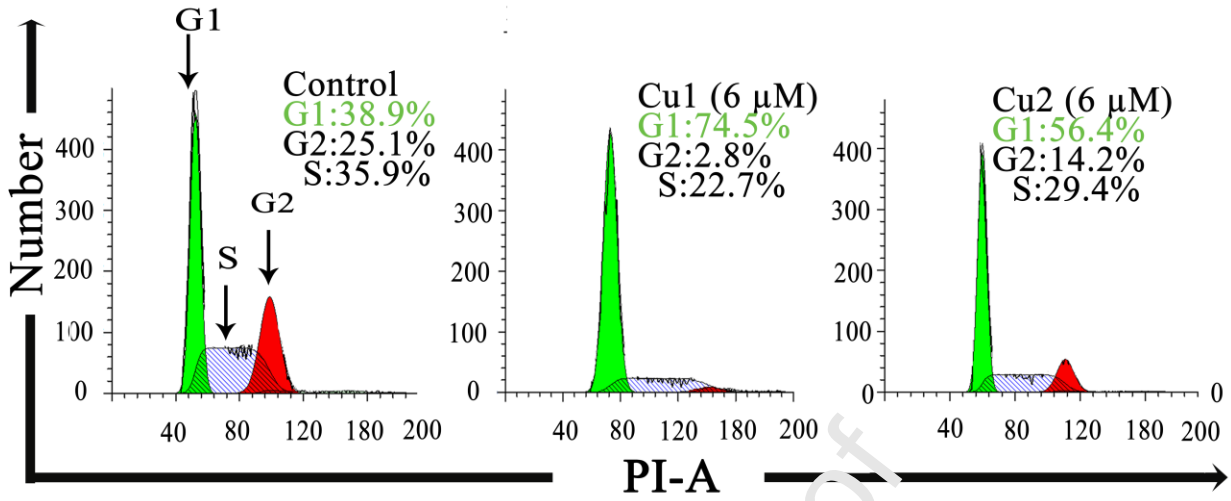

Fig. 6

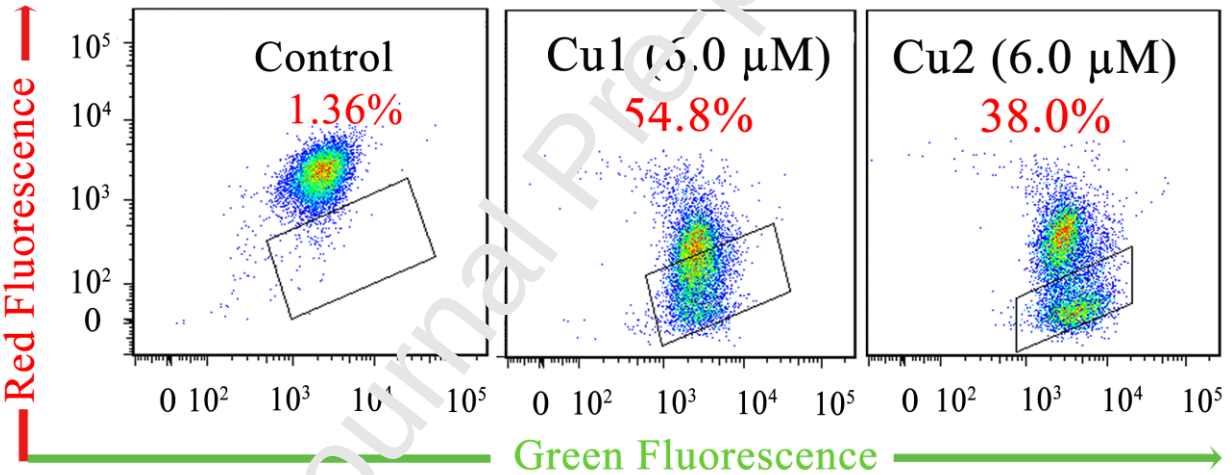

Fig. 7

Journal Pre-proof

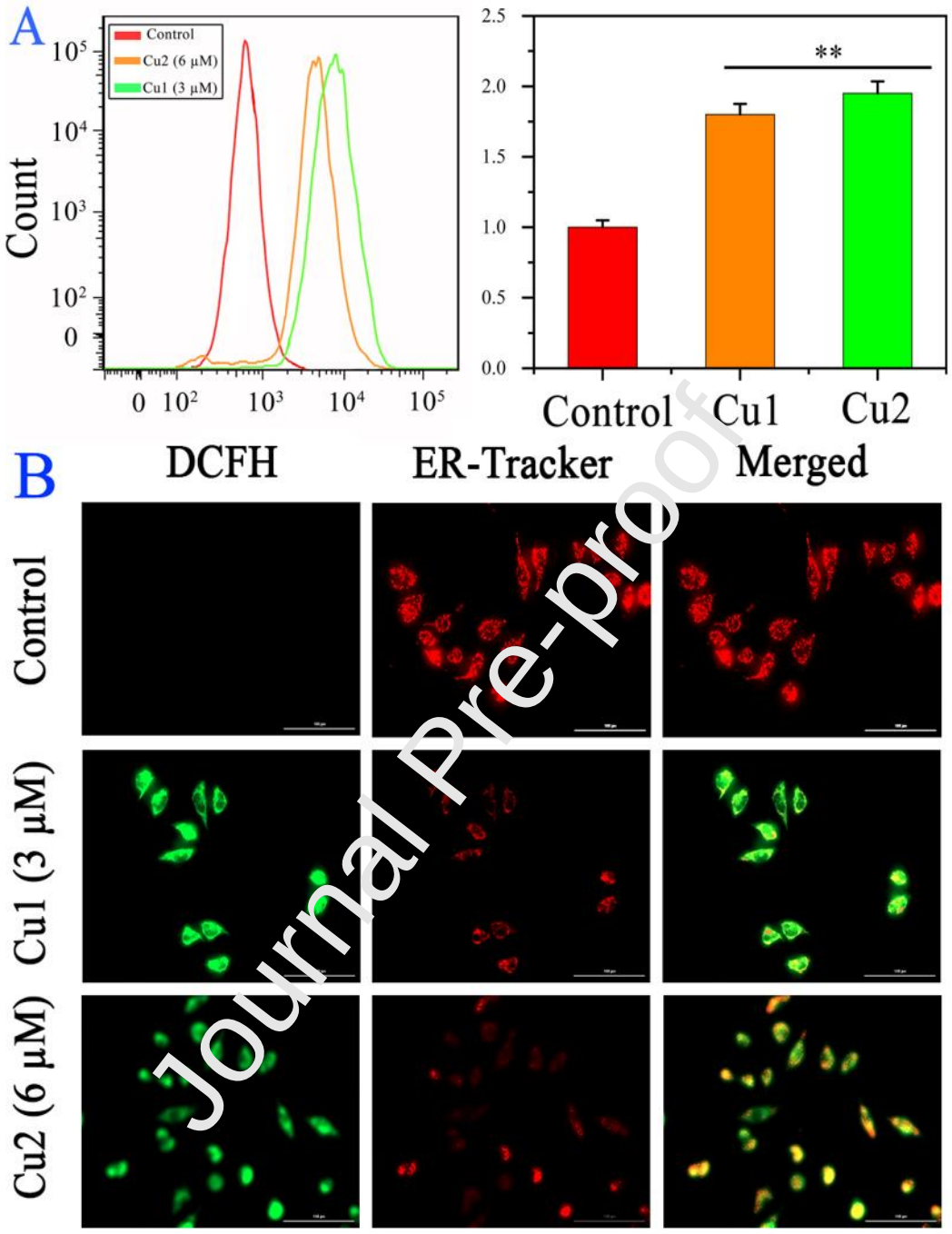

Journal Pre-proof

Fig. 8(A, B)

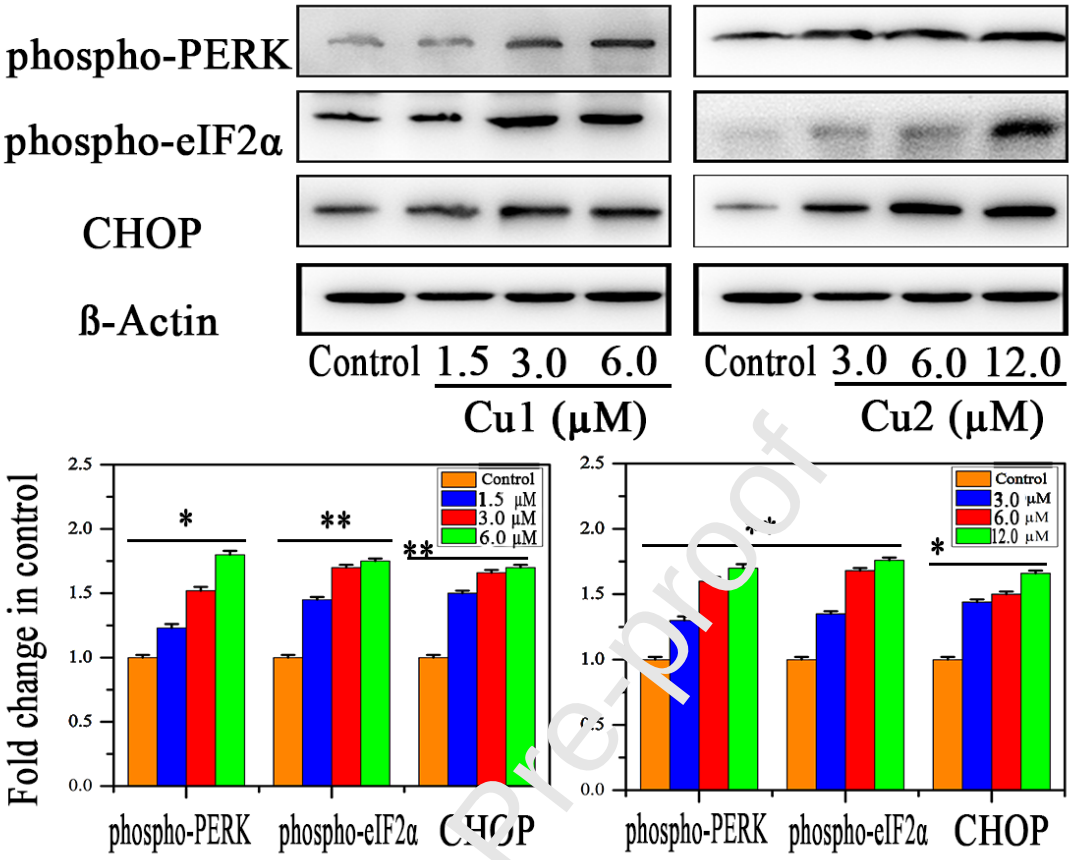

Fig. 9

Journal Pre-proof

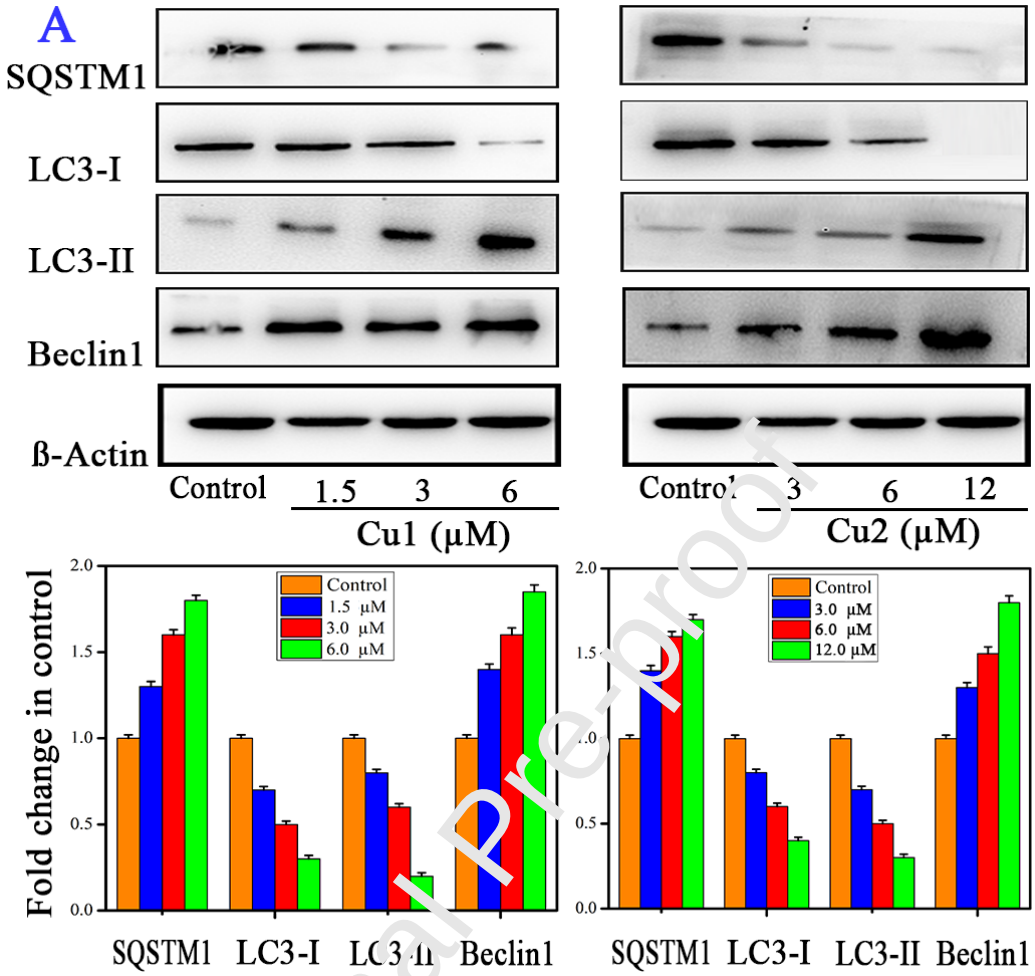

Fig. 10(A)

Journal Pre-proof

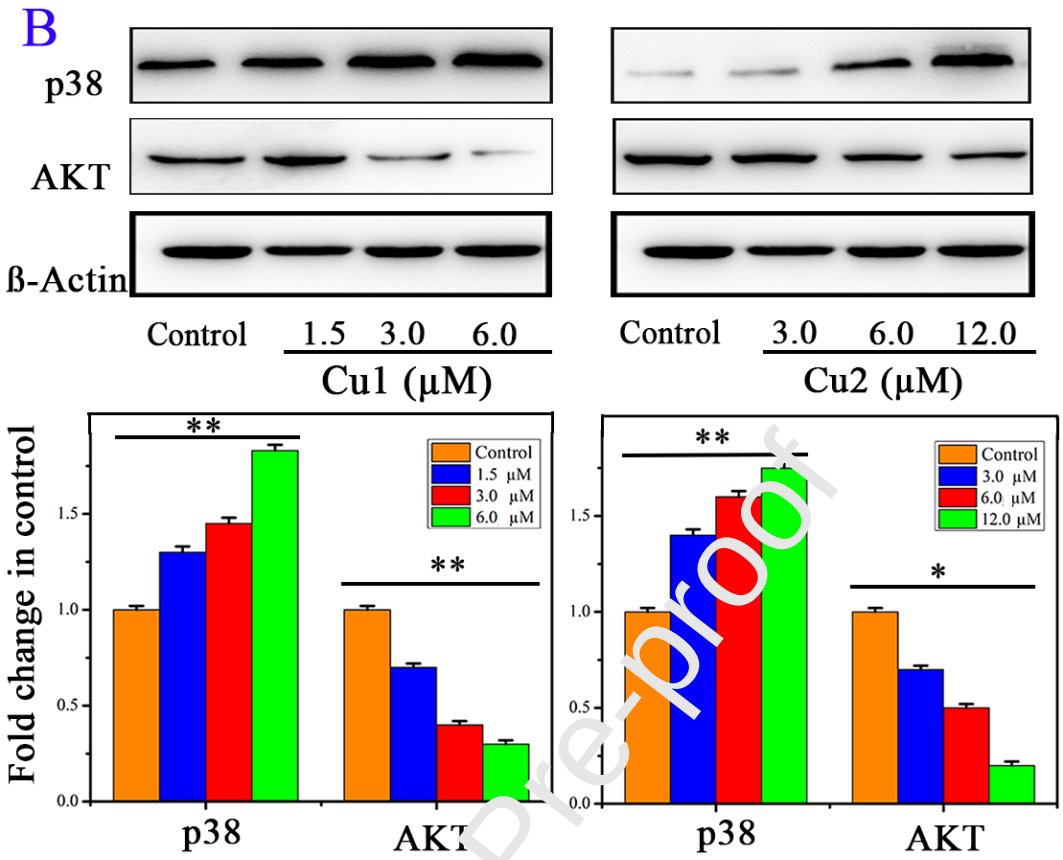

Fig. 10(B)

Journal Pre-proof

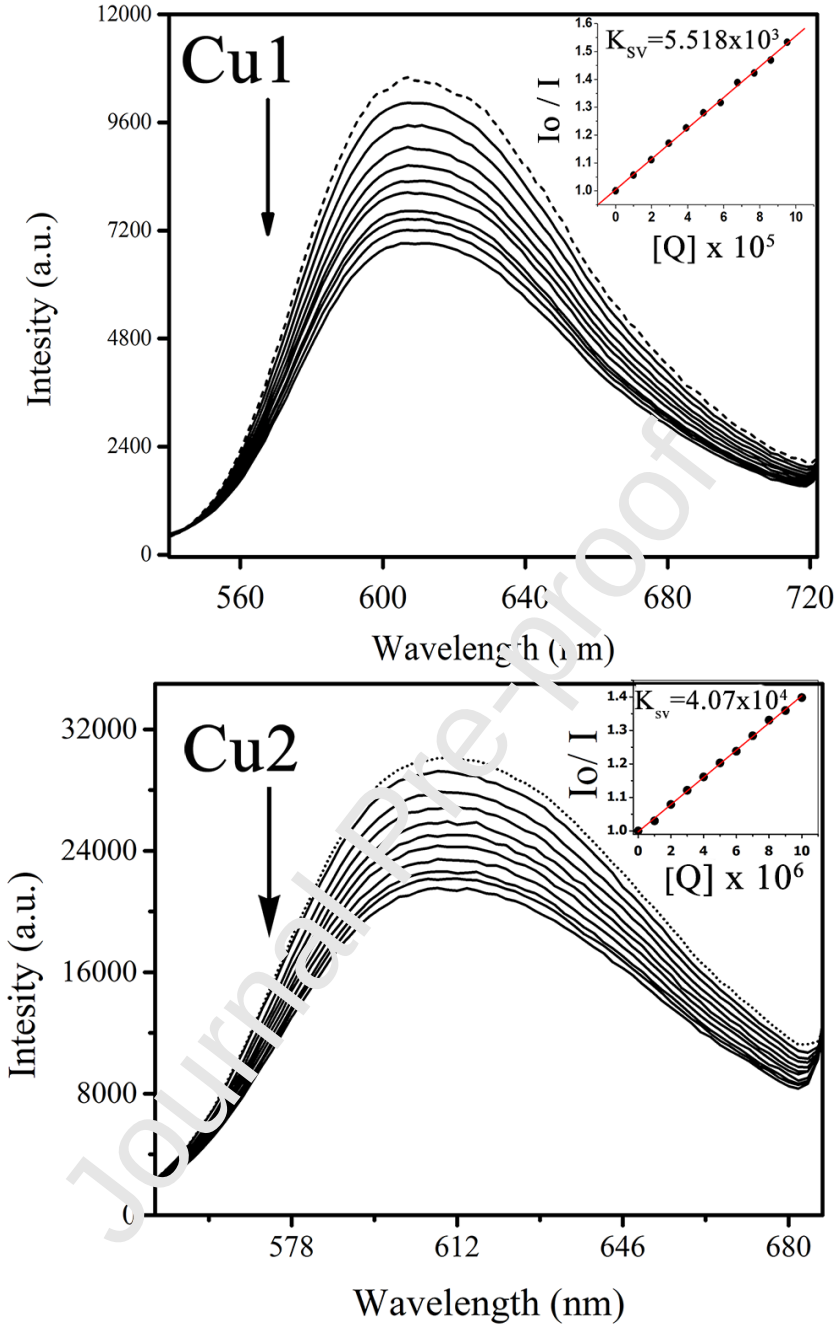
Cu1
Intesity (a.u.)
Wavelength (nm)
K_{SV}=5.518x10^3
Io / I
[Q] x 10^5
Cu2
Intesity (a.u.)
Wavelength (nm)
K_{SV}=4.07x10^4
Io/ I
[Q] x 10^6

Fig. 11

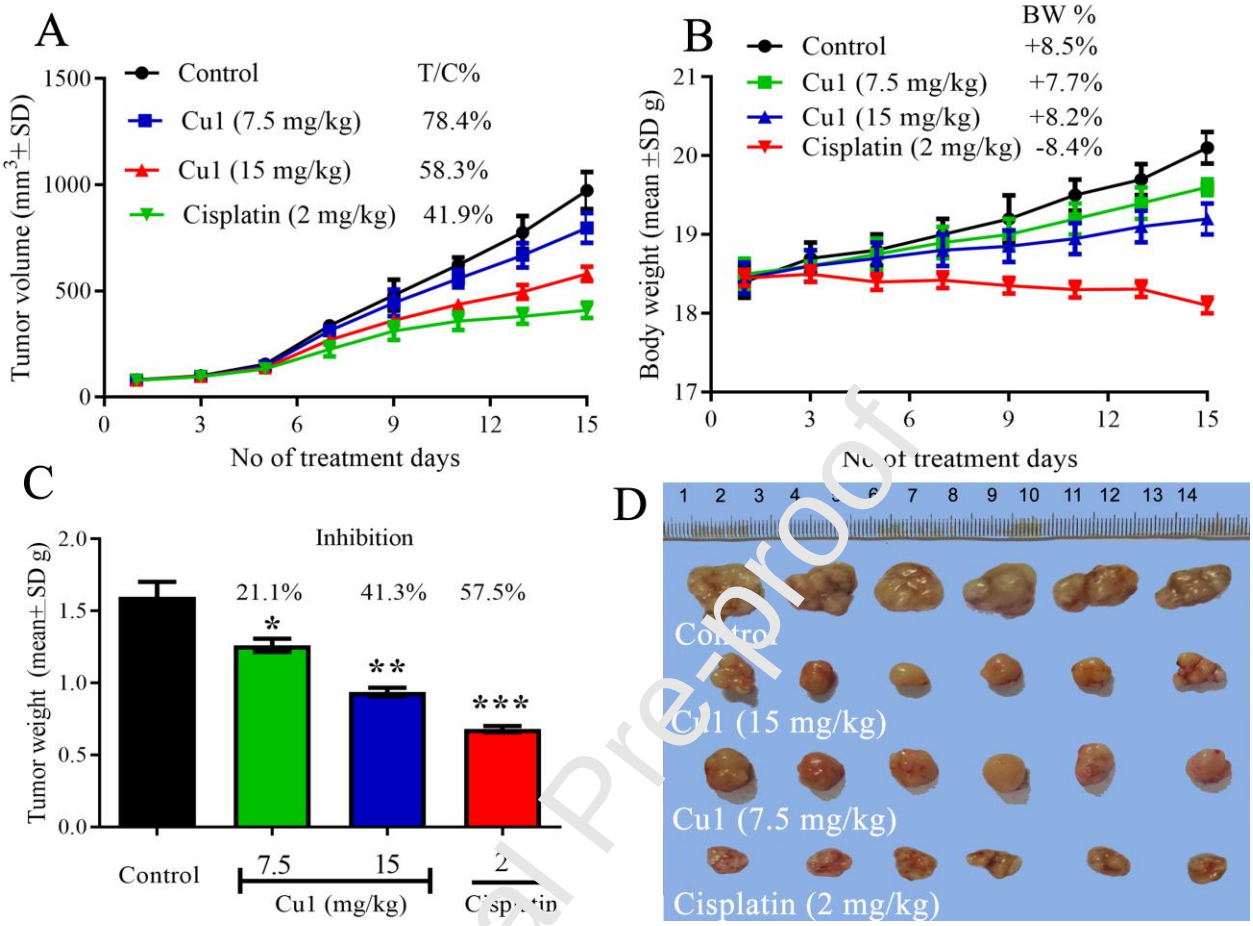

Fig. 12

Journal Pre-proof

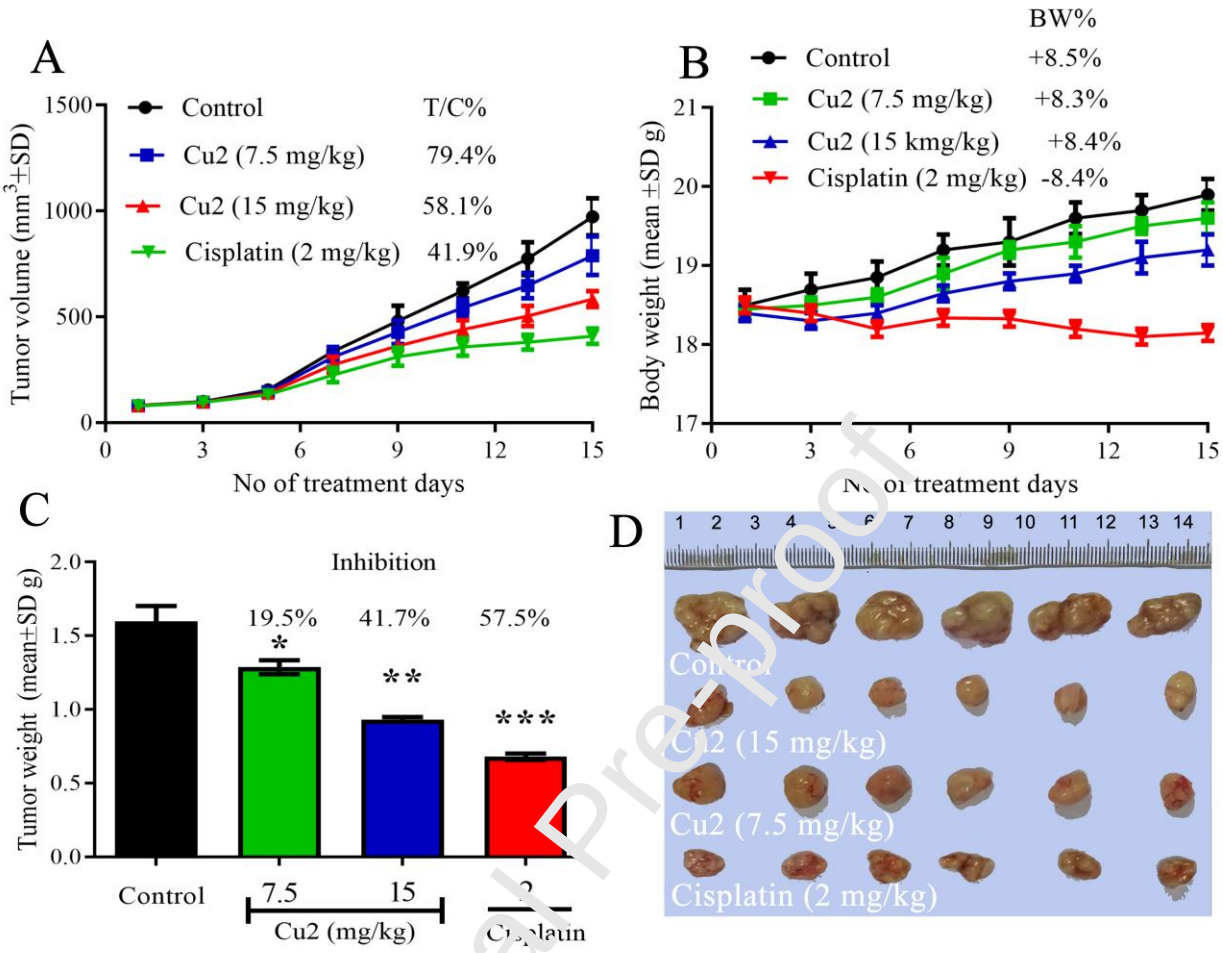

Fig. 13

Journal Pre-proof

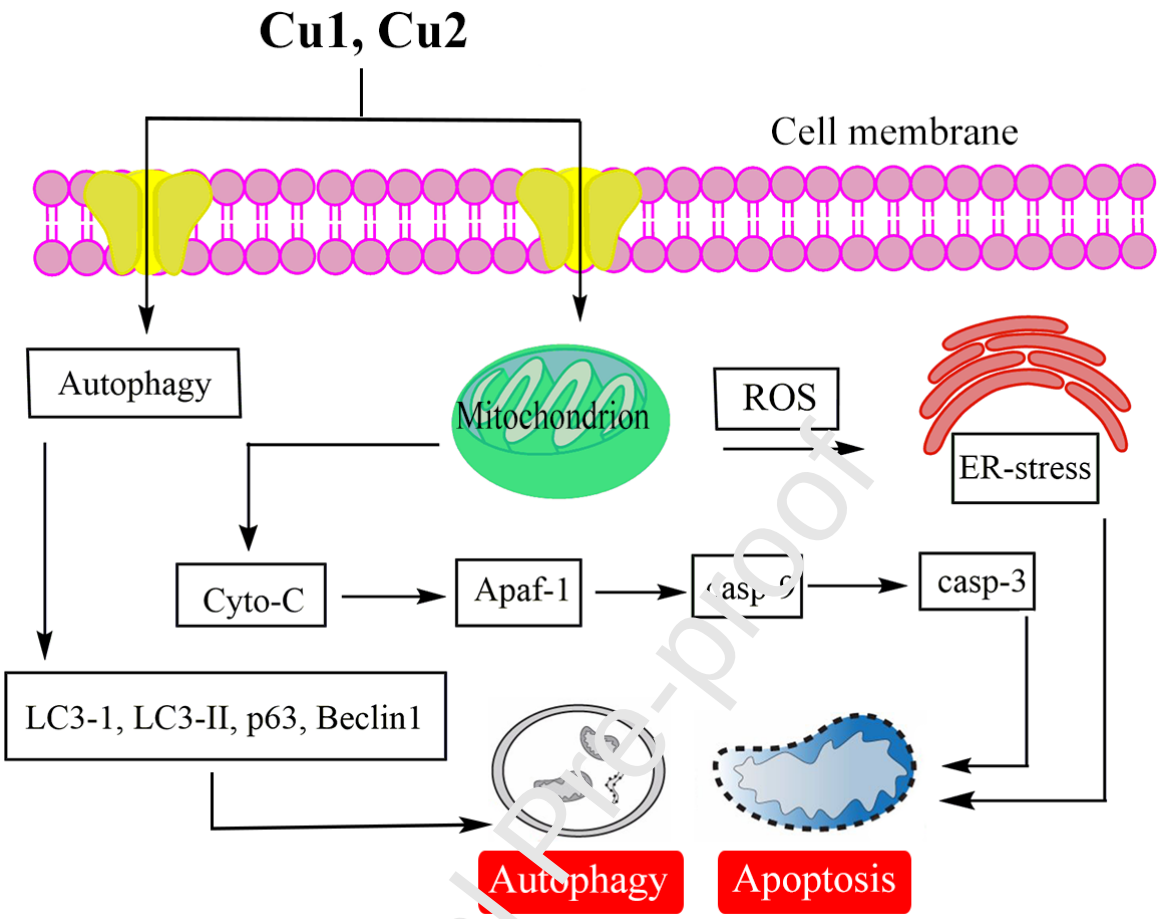

Fig. 14

Journal Pre-proof

Declaration of Interest Statement

All authors declare no conflict of interest for this work.

Journal Pre-proof

Graphical Abstract

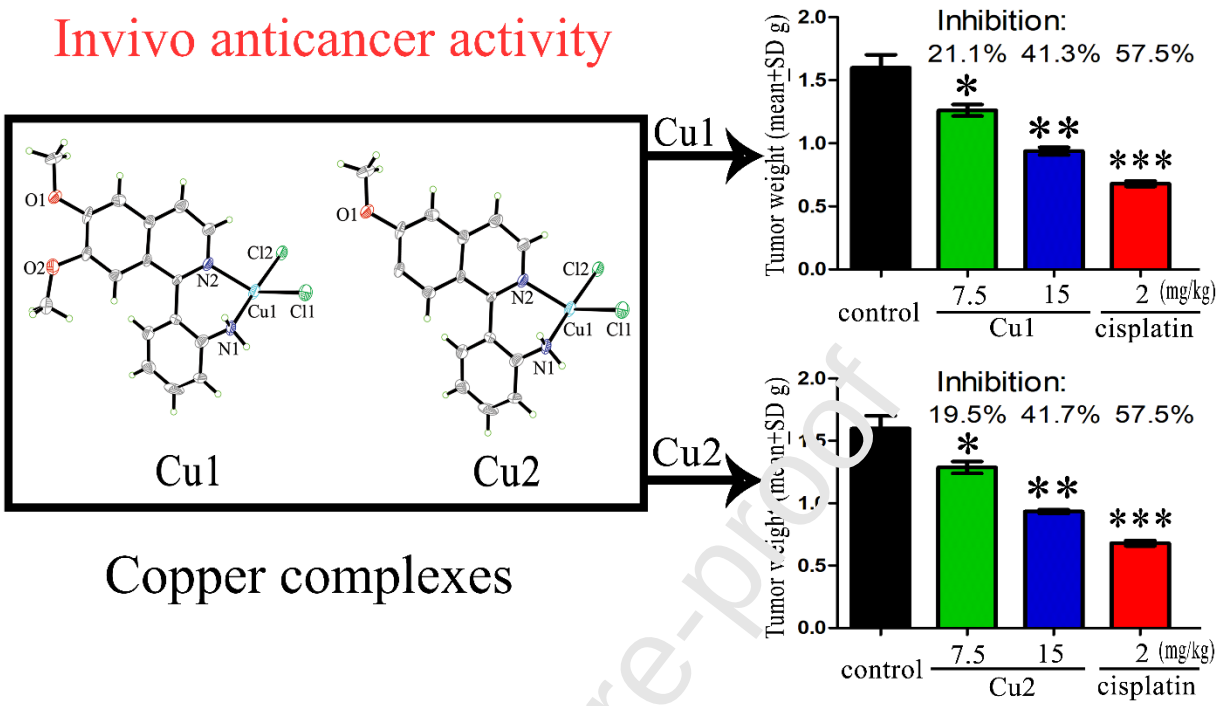

Cu1 [CuL^1Cl_2, L^1 = 2-(6,7-dimethoxyisoquinolin-1-yl) aniline] and **Cu2** [CuL^2Cl_2, L2 = 2-(6-methoxyisoquinolin-1-yl) aniline] induced bimodal death through apoptosis and autophagy in A549 cancer cells, and effectively inhibited the tumour growth in a xenografted mouse model bearing A549 cells but exhibited lower in vivo toxicity than cisplatin.

Journal Pre-proof

Highlights:

- Cu1 [CuL^1Cl_2, L^1 = 2-(6,7-dimethoxyisoquinolin-1-yl) aniline] was synthesized.
- Cu2 [CuL^2Cl_2, L^2 = 2-(6-methoxyisoquinolin-1-yl) aniline] was synthesized.
- Cu1 and Cu2 exhibited selective cytotoxicity on A549 via apoptosis and autophagy.
- Cu1 and Cu2 repressed tumor growth in xenograft mouse model of A549 cells.
- Cu1 and Cu2 arrested the cell cycle at G1-phase and activated caspases-3, -8 and -9.

Journal Pre-proof